This is the peer reviewed author accepted manuscript (post print) version of a published work that appeared in final form in:

Lu, Yi, Wang, Xiang, Fan, Deqi, Yang, Hang, Xu, Haolan, Min, Huihua & Yang, Xiaofei 2020 'Biomass derived Janus solar evaporator for synergic water evaporation and purification', *Sustainable Materials and Technologies* vol. 25, article no. e00180, pp. 1-10

This output may not exactly replicate the final published authoritative version for which the publisher owns copyright. It is not the copy of record. This output may be used for non-commercial purposes. This version is licensed under a Creative Commons CC-BY-NC-ND 4.0 license (http://creativecommons.org/licenses/by-nc-nd/4.0/).

The final definitive published version (version of record) is available at:
https://doi.org/10.1016/j.susmat.2020.e00180

Persistent link to the Research Outputs Repository:
http://researchoutputs.unisa.edu.au/11541.2/143377

General Rights
Copyright and moral rights for the publications made accessible in the Research Outputs Repository are retained by the authors and/or other copyright owners and it is a condition of accessing publications that users recognize and abide by the legal requirements associated with these rights.

- Users may download and print one copy for the purpose of private study or research.
- You may not further distribute the material or use it for any profit-making activity or commercial gain
- You may freely distribute the persistent link identifying the publication in the Research Outputs Repository

If you believe that this document breaches copyright please contact us providing details, and we will remove access to the work immediately and investigate your claim.

Biomass Derived Janus Solar Evaporator for Synergic Water Evaporation and Purification

Abstract: Solar steam generation has been regarded as an environment-friendly strategy to mitigate the worldwide freshwater shortage. Challenges remain in terms of high-cost of raw materials, complicated fabrications and inability to scale up. Here, an all biomass loofah-derived evaporator composed of a porous supporter (alkalized loofah sponge) and light absorber (carbonized loofah sponge) for highly efficient solar steam generation is proposed, which employs synergistic concepts of solar evaporation and surface biosorption for simultaneous generating freshwater and recycling heavy-metal ions. This multifunctional photothermal evaporator shows an excellent evaporation rate of 1.36 kg m^{-2} h^{-1} and corresponding light-to-vapor energy conversion efficiency of 83.7 % under 1.0 Sun, and simultaneously delivers excellent self-desalting performance. The developed photothermal evaporator derived from biomass loofah is promising for low-cost and large-scale freshwater production for the water-stressed regions.

Keywords: solar steam generation; biomass; photothermal material; water purification

1. Introduction

Given the critical issue of global clean water scarcity threatening human health and survival, it is necessary to develop a technology to use readily available renewable resources, e.g. solar energy and seawater to produce clean water. Solar thermal water evaporation, as a reliable and efficient solar energy related approach, has attracted enormous attention due to its advantage of sustainability and environmentally friendliness [1-5]. The recently developed interfacial solar steam generation paves the way for using solar energy for freshwater production. Highly efficient solar steam generation relies on the design and development of high-performance solar-thermal conversion materials, which focus on the amelioration of solar absorptance, heat localization, water transportation, and quick vapor escape [6-11]. Many photothermal materials have been developed to involve in solar steam generation, including plasmonic nanoparticles [12-16], carbon-based materials [17-21], polymers [22-27], semiconductors [28-34] and so on. However, to push forward the real-world applications, preparation of photothermal materials with low cost, excellent stability, environmental friendliness and scalability is still highly demanded. The conversion of biomass waste into value-added photothermal materials offers an ideal solution.

Currently, various evaporators originated from plants and/or plant parts have been exploited for solar steam generation due to low cost, low toxicity as well as excellent physical and chemical stabilities [35-38]. For instance, a series of wood-based solar evaporators with elaborated designs were developed for highly efficient solar desalination [39-44]. Carbonized mushroom was surprisingly found to be an excellent solar steam generation device with an efficiency of 78% under 1.0 sun illumination [45]. Tan's group demonstrated a sustainable method of repurposing food waste as porous carbon-based solar evaporator for low-cost solar desalination [46]. Beyond these, many other biomass-derived solar evaporators were also prepared,

such as carbonized carrot [47], used cigarette filters [48] and wasted rice straw [49]. Accordingly, the economic and environmentally friendly biochar is a prominent solar evaporator candidate for solar steam generation device. However, the water evaporation rates of the biochar-derived evaporators still need to be further enhanced to push forward the real-world application.

Fabrication of elaborately designed porous structures is of great importance to promote thermal management and water transportation during solar steam generation [50-52], while the cost and feasibility in large scale production is still a vital practical issue need to be addressed. Loofah is a vigorous growing, high yield and widespread reticular fibrous plant, which possesses natural porous structures with outstanding mechanical strength. In many regions, it is used as natural dishwashing and bath sponge. Recently, loofah-sponge derived carbon materials have been investigated as environmental friendliness electromagnetic wave absorbing materials and photocatalysis materials. Lightweight carbonized loofah sponge/$CoFe_2O_4$ composites exhibited a high micro-wave absorbing performance, ascribing to the dielectric lotus-root-like carbon substrate. [53] Li et al. designed SiC-coated carbonized loofah sponge materials with polymer-like thermal insulation, outstanding electromagnetic shielding properties and flexural strength. [54] In addition, Fang's group has also successfully synthesized SnS_2/carbonized loofah sponge for effective photocatalytic heavy metal ions removal owing to the large specific surface of 3D hierarchical macroporous composites. [55] Therefore, carbonized loofah sponge has a potential to be chose as a continuous and porous 3D network carbon sponge, facilitating its applications for solar driven water transpiration.

Herein, we proposed a facile strategy to fabricate loofah-derived porous biochar as a solar evaporator via the carbonization process, which embraced the favorable hydrophilicity, high light absorptance in a broad spectrum, excellent scalability and low cost. As a result, the carbonized loofah together with an alkalized loofah can achieve a high evaporation rate of 1.36 kg m^{-2} h^{-1} under 1.0 sun, delivering an energy efficiency of 83.7%. Furthermore, an all loofah sponge-based evaporator composed of alkalized loofah sponge as thermal insulator and carbonized loofah sponge as light

absorber was designed, which brought dual functions of solar evaporation and heavy-metal ions absorption. This endows the loofah sponge-based evaporator prodigious prospects for efficient freshwater production without further stressing the environment.

2. Experimental Section

2.1 Fabrication of Carbonized Loofah Evaporators

Loofah purchased from local market was cut into pieces (10 × 10 cm). Then, they were soaked in ethanol and deionized water to remove soluble organic and inorganic substances. Alkalized loofah (AL) was prepared by immersing pieces of loofah in sodium hydroxide solution (10 wt%) at 80 ^{o}C for 2 h to remove lignin. Carbonized loofah (CL) sponge was obtained by calcination in N_2 for 2 h at 500, 600, 700 and 800 ^{o}C, and accordingly, the obtained samples were named as CL-500, CL-600, CL-700 and CL-800. Bacterial cellulose solution (BC, 0.5% solid content) was also implemented to fabricate a solar evaporator hydrogel based on CL-500 powders. Firstly, a certain amount of carbonized loofah powders was suspended in BC solution by constantly stirring for 10 min. Then the mixture was filtered into a film by a vacuum filtration strategy. The film was named as CL+BC sample.

2.2 Material Characterization

The crystal phases of the samples were investigated by X-ray diffraction using Cu Kα radiation (XRD, Ultima IV, Rigaku, Japan). Raman spectra characterization were carried out on a Raman microscope by using a Themor DXR532 780 nm semiconductor laser. The chemical compositions of samples were investigated by X-ray photoelectron spectroscopy (XPS) via Thermo VG Scientific ESCALAB 250 spectrometer. The XPS spectra was analyzed using the curve-fitting program (XPS Peak software). All the corresponding binding energies were calibrated by using the reference carbon C 1s at 284.6 eV. Fourier-transform infrared (FTIR, VERTEX 80V, Bruker, Germany) spectra were measured from 4000 to 400 cm^{-1} at room temperature. The hydrophilicity of the samples was investigated with a contact angle meter

(KRUSS, DSA100) by dropping water (15.0 μL) droplets on the surface of sample. The light absorption of loofah sponge before and after carbonization were measured using an ultraviolet–visible–near-infrared spectrophotometer attached with an integrating sphere. The infrared emissivity of the samples was determined by the infrared reflection spectra (2.5 – 15 μm) obtained by a FTIR spectrometer assembled with a golden integrating sphere (Frontier, PerkinElmer LLC). The solar absorptance (α) and thermal emissivity (ε) can be calculated by the following equations based on the measured reflectivity (Fig. S1),

$$\alpha = 1 - R(\lambda) - T(\lambda) = \frac{\int_{300} \cdots}{\int_{2500} \cdots} \quad (1)$$

$$\varepsilon = 1 - \alpha = 1 - \frac{\int \cdots \cdot sun(\cdots) \cdots}{\int \cdots} \quad (2)$$

where $R(\lambda)$ is the reflectivity function of the sample at different wavelength (λ), $T(\lambda)$ is zero as the sample is opaque, $I(\lambda)$ is the light intensity function of the solar spectrum at different wavelength (λ). Due to the solar spectrum is not uniformly distributed, the integral computation of α and ε are more effective.

2.3 Solar Evaporation Measurements

To comprehensively test the solar evaporation and energy conversion efficiency, a solar simulator (CEL-PE300L-3A, CEAULIGHT, Beijing, China) with an AM1.5 optical filter was used as the light source. Different magnification fresnel lens were assembled with the solar simulator to adjust the incident solar intensity. A Solar Power Meter (CEL-NP2000, CEAULIGHT, China) was used to measure and calibrate the light intensity. Once the solar simulator is on, the real-time weight loss was tracked by a high-accuracy electronic analytical balance (FA2004, 0.0001 g in accuracy) connected to a computer (with RS 232C serial ports). The evaporation rate was calculated by the mass change versus time curves. Simultaneously, infrared (IR) camera (FLIR E8) and thermocouple were employed to record the temperature of the evaporator surface. All experiments were implemented at the ambient temperature of ~25 °C, and the relative humidity of 40 ± 5%. The concentrations of Na^+, Pb^{2+}, Cu^{2+}

and Cr^{3+} in water and the content of Cr^{3+} absorbed by alkaline loofah were measured by an inductively coupled plasma-mass spectrometry (ICP-MS, NeXion 300X, Perkin Elmer Instruments, 0.1 $mg \cdot L^{-1}$ in accuracy).

3. Results and Discussion

The preparation procedure of carbonized loofah (CL) sponge used for solar evaporation is exhibited in Scheme 1 and Fig. S2. The original loofah (Fig. S2a) was cut into slices, compressed (Fig. S2b) and treated with NaOH to remove the lignin, resulted in AL (Fig. S2c, d, e). Then the AL was carbonized in a furnace with the protection of N_2 gas. After carbonization, the color of the loofah sponge turned from canary yellow to black (Fig. S2f). The obtained CL inherited the porous structure and light weight of the loofah sponge so that it can be supported by leaves (Scheme 1). Apart from the porous structure, hydrophilic surface is another required characteristic for water transportation from the bottom to the heated evaporation surface during solar steam generation. The original loofah is slightly hydrophobic and can float on the water surface (Fig. S3). After NaOH treatment, the obtained AL became hydrophilic (Fig. 2a). It is clear that the CL-500 sponge retained its hydrophilicity after carbonization, due to the major components of cellulose and polysaccharide chains. Compared with the AL whose surface swelled and deformed when it was in contact of water, the CL-500 sponge retained its shape and structure well when a water droplet penetrated the porous structure. Although the entire volume of the loofah sponge shrunk by about 30% after carbonization (Fig. 2b), the porous network and structure of fiber were well reserved as confirmed by optical microscopy images (Fig. 2c and 2d, Fig. S4). Figure 2e also exhibits the fibrous and interlaced microstructure of carbonized loofah sponge. The highly porous structure of the CL sponge can be clearly observed, which can serve as expressways for water transportation as well as the channels for rapid vapor escape.

In order to investigate the phase and crystalline structure of CL sponge, XRD spectra of the CL obtained at different calcination temperatures were recorded (Fig. 3a). It can be seen that all XRD patterns presented a distinct broad diffraction peak at ~26°, corresponding to (002) graphitic plane, which revealed the disordered amorphous carbon structure.[54] Meanwhile, the weak and broad peak at 42° evidenced the low degree of crystallinity of the CL sponge. The above results were further verified by the Raman spectra (Fig. 3b). The Raman peaks at 1340 cm^{-1} and 1590 cm^{-1} can be attributed to the disorder D-band of amorphous carbon and the in-plane sp^2 vibration of graphite crystal G-band, respectively. As a sign for the degree of graphitization, the D/G value of CL-500, CL-600, CL-700 and CL-800 is 1.28, 3.40, 2.06, and 0.67, indicating a higher content of amorphous carbon of CL sponges except the CL-800. XPS analysis was employed to confirm the chemical composition of CL-500, which revealed that the major elements were C and O (Fig. 3c). The strong C−C peak located at 284.8 eV suggested the deoxidation reactions took place during carbonization process (Fig. 3d). In addition, the functional group of the CL sponge were analyzed by FTIR spectroscopy (Fig. 3e). The characteristic absorption peaks at 633, 1620 and 1743 cm^{-1} can be assigned to hydroxyl and carboxylate groups. Except the CL-800, other CL sponges featured a C–O stretching peak at 1124 cm^{-1}, revealing that they all have a high content of oxygen-containing functional groups. The peaks at 3415 cm^{-1} and 1047 cm^{-1} corresponding to N–H/O-H and C–N were also observed, further confirming the hydrophilic nature of CL sponge. In order to achieve a high solar evaporation efficiency, high sunlight absorption is required. The solar absorption spectra (Fig. 3f) revealed the light absorption capability of the natural loofah sponge and CL sponges over the wavelength range of 750−2000 nm. Weighted by the standard air mass 1.5 global (AM 1.5 G) solar spectrum, the average integrated absorption of natural loofah sponge in the UV-Vis-infrared regions is only 40%. In contrast, the CL sponges showed a high absorption of 84%. Furthermore, almost 92% of the incident light can be absorbed by the wet CL-500, indicating a high light harvesting during solar steam generation. The enhancement of solar absorption for wet surfaces can be ascribed to the extra light absorptivity by

water in porous structure. Considering the energy consumption for the carbonization and its tiny influences on the solar absorption, the CL-500 sponge was selected and utilized as photothermal material for solar steam generation.

By integrating the CL-500 sponge with a thermal insulator of polystyrene (PS) foam wrapped with air-laid paper, a self-floating photothermal evaporator with a 2D water path was established (Fig. 4). This design is able to continuously transfer water to the evaporation surface while minimize the heat conduction loss during solar steam generation [56]. For comparison, solar evaporation with sole CL-500 sponge was also measured to elucidate the superiority of this design (Fig. 5). To systematically evaluate the evaporation performance of the CL+PS evaporator, the surface temperature and weight loss of water under various solar illuminations were recorded. Upon sunlight irradiation, the surface of the CL-500 absorbed the sunlight and generated localized heat on the surface quickly. The temperature of the CL-500 surface rapidly increased through light-to-heat conversion and drove the water evaporation thereof. Conspicuously, the steady surface temperature increased with the increment of solar intensity, which was nearly 38.3, 62.1, 53.4, 72.9 ^{o}C under 1.0, 3.0, 5.0 and 7.0 Sun separately, as recorded by the IR imaging (Fig. 4a). After 1 h solar steam generation under 1.0 Sun, the temperature of the bulk water was maintained to 25.2 ^{o}C, confirming that the heat converted from the light was effectively localized on the CL sponge surface and consumed by the water evaporation thereof. When the light intensity increased to 3.0 Sun, vapor can be clearly observed (Fig. 4a). Meanwhile, the evaporated water can be rapidly replenished via capillary action because of the negative pressure on the top of hydrophilic surface during evaporation. Compared to the ubiquitous natural water evaporation, the solar evaporation over the CL+PS evaporator was much faster (Fig. 4b). Due to the excellent photothermal effect, low thermal conduction loss, larger evaporating areas and porous microstructures, the evaporation rates of the CL+PS evaporator under 1.0, 3.0, 5.0 and 7.0 Sun were 1.38, 4.26, 6.83 and 9.81 kg m^{-2} h^{-1} respectively, while the evaporation rate of pure water under 1.0 sun was only 0.35 kg m^{-2} h^{-1}. In contrast, the sole CL-500 sponge without PS underneath owned a lower evaporation rate of 7.69 kg m^{-2}

h^{-1} (7.0 Sun) than that of CL+PS evaporator, due to the thermal loss to bulk water in absence of insulator foam evidenced by IR images (Fig. 5, Fig. S5).

The energy conversion efficiency (η) of solar evaporation can be calculated by

$$\eta=(v_e h_{PC})/(C_{opt} q_{in}) \quad (3)$$

where v_e is the net evaporation rate with dark evaporation deducted (0.13 kg m^{-2} h^{-1}), and $C_{opt}q_{in}$ is the power density of solar illumination (kW m^{-2}), and h_{PC} is the total phase change enthalpy described in Fig. S6 (kJ kg^{-1}), which can be estimated as

$$h_{PC} = \lambda_{Lh} + C_p \Delta T \quad (4)$$

$$\lambda_{Lh} = 1918.46 \times [T_0/(T_0\text{-}33.91)]^2 \quad (5)$$

where λ_{Lh} is the latent heat of water evaporation under the standard atmosphere pressure (kJ kg^{-1}), C_p represents the specific heat capacity of bulk water (4.18 kJ kg^{-1} K^{-1}), and ΔT is the temperature variation during the evaporation process (K). Therefore, the corresponding solar-to-vapor energy efficiency were calculated to be 85.5%, 94.7%, 93.4%, 95.7% under 1.0, 3.0, 5.0 and 7.0 Sun (Fig. 4c). The energy efficiency of the CL-500 sponge is comparable to many of the reported carbonized materials (Table 1). The energy balance between solar input and the energy loss was analyzed to verify the energy efficiency. The thermal loss during evaporation is comprised of thermal radiation, convection and conduction loss, which can be calculated by the following equations, [57]

$$Q_{radiation} = A_{pro}\, \varepsilon\sigma\, (T_0^4 - T_1^4) \quad (6)$$

$$Q_{\text{convection}} = A_{pro}\, h\, (T_0 - T_1) \quad (7)$$

$$Q_{\text{conduction}} = C_p m\, (T_3 - T_2) \quad (8)$$

Where A_{pro} is evaporation surface area (7 cm^2), ε is the infrared emissivity coefficient (0.8), σ is the Stefan-Boltzmann constant (5.6×10^{-8} W m^{-2} K^{-4}), h is the convection heat transfer coefficient (5 W m^{-2} K^{-1}), m is the weight of bulk water (69.1 g), T_0, T_1, T_2 and T_3 denote the average temperature of evaporator (38.3 °C), the temperature of ambient environment (25 °C), and the initial (23.9 °C) and final temperatures (25.2 °C) of bulk water. Therefore, the thermal radiation loss, thermal convection loss and thermal conduction loss under 1.0 Sun were nearly 0.032 W, 0.031 W and 0.0017

W. The total energy loss was about 13.3 % of the input energy and was in acorrdrance with the caculated energy efficiency (85.5%).

To further illustrate the practical application of the CL-500 sponge for solar evaporation, the stability of the CL-500 sponge evaporator at 3.0 sun in 3.5 wt% NaCl solution was investigated (Fig. 4d). No apparent change in water evaporation rate over 10 cycles of evaporation (1 hour for each cycle) was observed. The anti-salt accumulation performance of the CL-500 sponge under 3.0 Sun was also observed in Fig. 4e. Only a small amount of salt was accumulated on the surface of CL-500 sponge after 10 h evaporation. However, the accumulated salt can be dissolved back into the bulk water again via diffusion when the light was off.[58] This result implies that in practical applications, the salt may accumulate on the CL-500 surface after one day of solar evaporation, but it will be re-dissolved at night, and the CL-500 sponge can be reused the next day without the need of any treatment (Fig. S7). Therefore, it is reasonable to claim that the CL-500 sponge possesses self-desalting ability for solar steam generation.

To pursue a more environmentally friendly and multifunctional evaporator, an all loofah sponge-based structure (namely CL+AL evaporator) was designed. The alkalized loofah (AL) was utilized to replace the PS which not only eliminated the risk of pollution caused by PS, but also introduced a new function of heavy metal absorption by the AL during solar steam generation (Fig. 6a). The solar evaporation rate and energy efficiency of CL+AL evaporator was measured to be 1.36 kg m^{-2} h^{-1} and 83.7% (Fig. 6b, c), which was slightly lower than that of the CL+PS evaporator (1.38 kg m^{-2} h^{-1}, 85.5%). This tiny sacrifice was hugely compensated by a new and impressive function, that was the AL sponge with rich pores can rapidly adsorb Cr^{3+} ions with a capacity of 7151 mg/kg evidenced by the ICP result. Moreover, the cost of all biomass based evaporator is estimated to be low ($1 per kg), implying its promising potential for scalable solar stem generation.

To further assess the potential of the CL-500 sponge in the application of wastewater treatment, various solutions of heavy-metal ions (Pb^{2+}, Cu^{2+}, Cr^{3+}, 5000 mg/L) were employed for solar evaporation. The concentrations of the heavy-metal

ions in the collected water (Fig. 7a) were all dramatically decreased (4 orders of magnitude) compared to those of the untreated water, which met the World Health Organization (WHO) drinking water standard (the dashed lines refer to (Pb^{2+}: 0.1 mg/L, Cu^{2+}: 0.1 mg/L, Cr^{3+}: 0.1 mg/L). Meanwhile, the desalination performance was estimated by evaporating simulated seawater (3.5 wt%, the average salinity of the world ocean), which revealed the concentration of Na^{+} in the collected water was 27.99 mg L^{-1}, much lower than the standard salinity level of the drinkable desalination-water of WHO. The solar absorption properties of used CL evaporator manifested the stable broad solar absorption properties of carbonized loofah sponge (Fig. 7b). Furthermore, it was demonstrated that the CL-500 evaporator can work well under the rigorous conditions, such as in acid (pH=1) and alkali (pH=14) solution (Fig. 7c). No degradation of the materials was observed. The PH value of collected water is neutral. Fig. 7d displayed the characteristic absorption peaks of both dye contaminated water (10 mg/L methyl orange (MO) and methylene blue (MB) solutions) and purified water. It is noticed that the all the collected water was colorless and the absorbance of purified water is close to zero, indicating extremely low concentration of the dyes. More importantly, outdoors performance was also examined (Fig. 8). A number of CL-500 evaporators were a neatly arranged side by side in the solar evaporation device, floating on the water surface. At noon of the winter weather (November, Nanjing, 12~13 ℃, 0.6~0.8 Sun), the vapor produced by the carbonized loofah sponge is spreading over the chamber, and then condensed as well as collected along the inclined wall to the condensing chamber. Considering that the AL and CL are all biomass derived materials which are cost effective and environmentally friendly, this advanced loofah sponge-based evaporator has showed great potential for the synergic applications of solar driven desalination and heavy metal ions adsorption.

4. Conclusion

A photothermal evaporator composed of AL and CL has been explored for low-cost, multifunctional and environmentally friendly solar steam generation. The

excellent light absorption, hydrophilicity, strong and reticular fibrous structure of the CL enabled highly efficient light-to-heat conversion and solar evaporation, while the AL rendered an impressive ability in rapid heavy-metal ions absorption. Upon 1.0 sun illumination, the CL+AL evaporator exhibited a high evaporation rate of 1.36 kg m^{-2} h^{-1} and energy conversion efficiency of 83.7%. The evaporator can not only produce clean water directly from the brine and dye polluted water but also adsorb heavy-metal ions from waste water. Such an all biomass loofah-based solar steam generation has shown great potential for real-world applications in desalination as well as industrial and domestic wastewater abatement, due to the low cost, environmental friendless and scalability of the raw materials. It also provides inspiration for the future development of fully biomass-based solar thermal evaporator.

Acknowledgements

This work was supported by the National Natural Science Foundation of China (21975129, 51902164), Natural Science Foundation of Jiangsu Province (BK20180777), Natural Science Foundation of Jiangsu Higher Education Institutions of China (18KJB430018), and Scientific Research Foundation for Advanced Talents (CXL2018046), Science Innovation Foundation for Young Scientists (CX2018012), Nanjing Forestry University, Australian Research Council (FT190100485). This work was also partially supported by Student's Platform for Innovation and Entrepreneurship Training Program in Jiangsu Province (201810298029Z), Student's Platform for Innovation and Entrepreneurship Training Program of Nanjing Forestry University (2018NFUSPITP602) and a project funded by the Priority Academic Program Development of Jiangsu Higher Education Institutions (PAPD).

References

[1] G. Ni, S.H. Zandavi, S.M. Javid, S.V. Boriskina, T.A. Cooper, G. Chen, A salt-rejecting floating solar still for low-cost desalination, **Energy** Environ. Sci. 11(6) (2018) 1510-1519.

[2] M. Gao, L. Zhu, C.K. Peh, G.W. Ho, Solar absorber material and system designs for photothermal water vaporization towards clean water and energy production, **Energy** Environ. Sci. 12(3) (2019) 841-864.

[3] L. Zhou, X. Li, G.W. Ni, S. Zhu, J. Zhu, The revival of thermal utilization from the sun: Interfacial solar vapor generation, Natl. Sci. Rev. 6(3) (2019) 562-578.

[4] C. Chen, Y. Kuang, L. Hu, Challenges and opportunities for solar evaporation, Joule 3(3) (2019) 683-718.

[5] G. Xue, Q. Chen, S. Lin, J. Duan, P. Yang, K. Liu, J. Li, J. Zhou, Highly efficient water harvesting with optimized solar thermal membrane distillation device, Global Challenges 2(5-6) (2018) 1800001.

[6] H. Ghasemi, G. Ni, A.M. Marconnet, J. Loomis, S. Yerci, N. Miljkovic, G. Chen, Solar steam generation by heat localization, Nat. Commun. 5 (2014) 4449.

[7] Y. Shi, R. Li, Y. Jin, S. Zhuo, L. Shi, J. Chang, S. Hong, K.-C. Ng, P. Wang, A 3D photothermal structure toward improved energy efficiency in solar steam generation, Joule 2(6) (2018) 1171-1186.

[8] Z. Liu, B. Wu, B. Zhu, Z. Chen, M. Zhu, X. Liu, Continuously producing watersteam and concentrated brine from seawater by hanging photothermal fabrics under sunlight, Adv. Funct. Mater. 24 (2019) 1905485.

[9] Y. Guo, X. Zhou, F. Zhao, J. Bae, B. Rosenberger, G. Yu, Synergistic energy nanoconfinement and water activation in hydrogels for efficient solar water desalination, ACS Nano 13(7) (2019) 7913-7919.

[10] X. Wu, G.Y. Chen, G. Owens, D. Chu, H. Xu, Photothermal materials: A key platform enabling highly efficient water evaporation driven by solar energy, Mater. Today Energy 12 (2019) 277-296.

[11] H. Su, J. Zhou, L. Miao, J. Shi, Y. Gu, P. Wang, Y. Tian, X. Mu, A. Wei, L. Huang, S. Chen, Z. Deng, A hybrid hydrogel with protonated g-C_3N_4 and graphene oxide as an efficient absorber for solar steam evaporation, Sustainable Mater. Technol. 20 (2019) e00095.

[12] L. Zhou, Y. Tan, J. Wang, W. Xu, Y. Yuan, W. Cai, S. Zhu, J. Zhu, 3D self-assembly of aluminium nanoparticles for plasmon-enhanced solar desalination, Nat. Photonics 10(6) (2016) 393-398.

[13] L. Zhou, S. Zhuang, C. He, Y. Tan, Z. Wang, J. Zhu, Self-assembled spectrum selective plasmonic absorbers with tunable bandwidth for solar energy conversion, Nano Energy 32 (2017) 195-200.

[14] X. Zhang, X. Wang, W.D. Wu, X.D. Chen, Z. Wu, Self-floating monodisperse microparticles with a nano-engineered surface composition and structure for highly efficient solar-driven water evaporation, J. Mater. Chem. A 7(12) (2019) 6963-6971.

[15] M. Gao, P.K.N. Connor, G.W. Ho, Plasmonic photothermic directed broadband sunlight harnessing for seawater catalysis and desalination, **Energy** Environ. Sci. 9(10) (2016) 3151-3160.

[16] Y. Liu, X. Wang, H. Wu, High-performance wastewater treatment based on reusable functional photo-absorbers, Chem. Eng. J. 309 (2017) 787-794.

[17] F. Wang, D. Wei, Y. Li, T. Chen, P. Mu, H. Sun, Z. Zhu, W. Liang, A. Li, Chitosan/reduced graphene oxide-modified spacer fabric as a salt-resistant solar absorber for efficient solar steam generation, J. Mater. Chem. A 7(31) (2019) 18311-18317.

[18] X. Yan, H. Li, J. Sun, P. Liu, H. Zhang, B. Xu, J. Guo, Pt nanoparticles decorated high-defective graphene nanospheres as highly efficient catalysts for the hydrogen evolution reaction, Carbon 137 (2018) 405-410.

[19] X. Wang, X. Li, G. Liu, J. Li, X. Hu, N. Xu, W. Zhao, B. Zhu, J. Zhu, An interfacial solar heating assisted liquid sorbent atmospheric water generator, Angew. Chem. Int. **Ed.** 58 (2019) 1-6.

[20] X. Wu, T. Gao, C. Han, J. Xu, G. Owens, H. Xu, A photothermal reservoir for highly efficient solar steam generation without bulk water, Sci. Bull. 64(21) (2019) 1625-1633.

[21] J. Zhou, Y. Gu, Z. Deng, L. Miao, H. Su, P. Wang, J. Shi, The dispersion of au nanorods decorated on graphene oxide nanosheets for solar steam generation, Sustainable Mater. Technol. 19 (2019) e00090.

[22] C. Tu, W. Cai, X. Chen, X. Ouyang, H. Zhang, Z. Zhang, A 3D-structured sustainable solar-driven steam generator using super-black nylon flocking materials, Small 15(11) (2019) 1902070.

[23] Z. Deng, L. Miao, P.-F. Liu, J. Zhou, P. Wang, Y. Gu, X. Wang, H. Cai, L. Sun, S. Tanemura, Extremely high water-production created by a nanoink-stained pva evaporator with embossment structure, Nano Energy 55 (2019) 368-376.

[24] C. Wang, Y. Wang, X. Song, M. Huang, H. Jiang, A facile and general strategy to deposit polypyrrole on various substrates for efficient solar-driven evaporation, Adv. Sustain. Syst. 3(1) (2019) 1800108.

[25] W. Li, Z. Li, K. Bertelsmann, D.E. Fan, Portable low-pressure solar steaming-collection unisystem with polypyrrole origamis, Adv. Mater. 31(29) (2019) e1900720.

[26] X. Wang, Q. Liu, S. Wu, B. Xu, H. Xu, Multilayer polypyrrole nanosheets with self-organized surface structures for flexible and efficient solar-thermal energy conversion, Adv. Mater. 31(19) (2019) e1807716.

[27] J. Jia, W. Liang, H. Sun, Z. Zhu, C. Wang, A. Li, Fabrication of bilayered attapulgite for solar steam generation with high conversion efficiency, Chem. Eng. J. 361 (2019) 999-1006.

[28] Z. Zhang, P. Mu, J. Han, J. He, Z. Zhu, H. Sun, W. Liang, A. Li, Superwetting and mechanically robust MnO_2 nanowire–reduced graphene oxide monolithic aerogels for efficient solar vapor generation, J. Mater. Chem. A 7(30) (2019) 18092-18099.

[29] R. Chen, X. Wang, Q. Gan, T. Zhang, K. Zhu, M. Ye, A bifunctional MoS_2-based solar evaporator for both efficient water evaporation and clean freshwater collection, J. Mater. Chem. A 7(18) (2019) 11177-11185.

[30] J. Wang, Y. Li, L. Deng, N. Wei, Y. Weng, S. Dong, D. Qi, J. Qiu, X. Chen, T. Wu, High-performance photothermal conversion of narrow-bandgap Ti_2O_3 nanoparticles, Adv. Mater. 29(3) (2017) 1603730.

[31] Y. Xu, J. Ma, Y. Han, J. Zhang, F. Cui, Y. Zhao, X. Li, W. Wang, Multifunctional cuo nanowire mesh for highly efficient solar evaporation and water purification, ACS Sustain. Chem. Eng. 7(5) (2019) 5476-5485.

[32] X. Wu, M.E. Robson, J.L. Phelps, J.S. Tan, B. Shao, G. Owens, H. Xu, A flexible photothermal cotton-CuS nanocage-agarose aerogel towards portable solar steam generation, Nano Energy 56 (2019) 708-715.

[33] Y. Lu, T. Dai, C. Lu, C. Cao, W. Zhang, W. Xu, H. Min, X. Yang, Fabrication of doped $SmBaCo_2O_{5+\delta}$ double perovskites for enhanced solar-driven interfacial evaporation, Ceram. Int. 45(18) (2019) 24903-24908.

[34] P. Wang, Y. Gu, L. Miao, J. Zhou, H. Su, A. Wei, X. Mu, Y. Tian, J. Shi, H. Cai, Co_3O_4 nanoforest/ni foam as the interface heating sheet for the efficient solar-driven water evaporation under one sun, Sustainable Mater. Technol. 20 (2019) e00106.

[35] H. Geng, Q. Xu, M. Wu, H. Ma, P. Zhang, T. Gao, L. Qu, T. Ma, C. Li, Plant leaves inspired sunlight-driven purifier for high-efficiency clean water production, Nat. Commun. 10(1) (2019) 1512.

[36] M. Zhu, Y. Li, G. Chen, F. Jiang, Z. Yang, X. Luo, Y. Wang, S.D. Lacey, J. Dai, C. Wang, C. Jia, J. Wan, Y. Yao, A. Gong, B. Yang, Z. Yu, S. Das, L. Hu, Tree-inspired design for high-efficiency water extraction, Adv. Mater. 29(44) (2017) 1704107.

[37] X. Zhao, H. Chen, F. Kong, Y. Zhang, S. Wang, S. Liu, L.A. Lucia, P. Fatehi, H. Pang, Fabrication, characteristics and applications of carbon materials with different morphologies and porous structures produced from wood liquefaction: A review, Chem. Eng. J. 364 (2019) 226-243.

[38] D.P. Storer, J.L. Phelps, X. Wu, G. Owens, N.I. Khan, H. Xu, Graphene and rice-straw-fiber-based 3D photothermal aerogels for highly efficient solar evaporation, ACS Appl. Mater. **Interfaces** 12(13) (2020) 15279-15287.

[39] Y. Kuang, C. Chen, S. He, E.M. Hitz, Y. Wang, W. Gan, R. Mi, L. Hu, A high-performance self-regenerating solar evaporator for continuous water desalination, Adv. Mater. 31(23) (2019) e1900498.

[40] S. He, C. Chen, Y. Kuang, R. Mi, Y. Liu, Y. Pei, W. Kong, W. Gan, H. Xie, E. Hitz, C. Jia, X. Chen, A. Gong, J. Liao, J. Li, Z.J. Ren, B. Yang, S. Das, L. Hu, Nature-inspired salt resistant bimodal porous solar evaporator for efficient and stable water desalination, **Energy** Environ. Sci. 12(5) (2019) 1558-1567.

[41] H. Liu, C. Chen, H. Wen, R. Guo, N.A. Williams, B. Wang, F. Chen, L. Hu, Narrow bandgap semiconductor decorated wood membrane for high-efficiency solar-assisted water purification, J. Mater. Chem. A 6(39) (2018) 18839-18846.

[42] H. Liu, C. Chen, G. Chen, Y. Kuang, X. Zhao, J. Song, C. Jia, X. Xu, E. Hitz, H. Xie, S. Wang, F. Jiang, T. Li, Y. Li, A. Gong, R. Yang, S. Das, L. Hu, High-performance solar steam device with layered channels: Artificial tree with a reversed design, Adv. Energy Mater. 8(8) (2018) 1701616.

[43] T. Li, H. Liu, X. Zhao, G. Chen, J. Dai, G. Pastel, C. Jia, C. Chen, E. Hitz, D. Siddhartha, R. Yang, L. Hu, Scalable and highly efficient mesoporous wood-based solar steam generation device: Localized heat, rapid water transport, Adv. Funct. Mater. 28(16) (2018) 1707134.

[44] X. Wu, G.Y. Chen, W. Zhang, X. Liu, H. Xu, A plant-transpiration-process-inspired strategy for highly efficient solar evaporation, Adv. Sustainable Syst. 1(6) (2017) 1700046.

[45] N. Xu, X. Hu, W. Xu, X. Li, L. Zhou, S. Zhu, J. Zhu, Mushrooms as efficient solar steam-generation devices, Adv. Mater. 29(28) (2017) 1606762.

[46] Y. Zhang, S.K. Ravi, S.C. Tan, Food-derived carbonaceous materials for solar desalination and thermo-electric power generation, Nano Energy 65 (2019) 104006.

[47] Y. Long, S. Huang, H. Yi, J. Chen, J. Wu, Q. Liao, H. Liang, H. Cui, S. Ruan, Y.-J. Zeng, Carrot-inspired solar thermal evaporator, J. Mater. Chem. A 7(47) (2019) 26911-26916.

[48] H. Sun, Y. Li, Z. Zhu, P. Mu, F. Wang, W. Liang, C. Ma, A. Li, Photothermal conversion material derived from used cigarette filters for solar steam generation, ChemSusChem 12(18) (2019) 4257-4264.

[49] Q. Fang, T. Li, Z. Chen, H. Lin, P. Wang, F. Liu, Full biomass-derived solar stills for robust and stable evaporation to collect clean water from various water-bearing media, ACS Appl. Mater. **Interfaces** 11(11) (2019) 10672-10679.

[50] Y. Ito, Y. Tanabe, J. Han, T. Fujita, K. Tanigaki, M. Chen, Multifunctional porous graphene for high-efficiency steam generation by heat localization, Adv. Mater. 27(29) (2015) 4302-7.

[51] J. Fang, J. Liu, J. Gu, Q. Liu, W. Zhang, H. Su, D. Zhang, Hierarchical porous carbonized lotus seedpods for highly efficient solar steam generation, Chem. Mater. 30(18) (2018) 6217-6221.

[52] X. Hu, J. Zhu, Tailoring aerogels and related 3D macroporous monoliths for interfacial solar vapor generation, Adv. Funct. Mater. (2019) 1907234.

[53] L. Liu, S. Yang, H. Hu, T. Zhang, Y. Yuan, Y. Li, X. He, Lightweight and efficient microwave-absorbing materials based on loofah-sponge-derived hierarchically porous carbons, ACS Sustain. Chem. Eng. 7(1) (2018) 1228-1238.

[54] S.T. Li, D.Y. Liu, W.C. Li, G.X. Sui. Strong and heat-resistant SiC-coated carbonized natural loofah sponge for electromagnetic interference shielding, ACS Sustain. Chem. Eng. 8 (2020) 435-444.

[55] L. Han, Y.L. Zhong, Y. Su, L.T. Wang, L.S. Zhu, X.F. Fei, Y.Z. Dong, G. Hong, Y.T. Zhou, D. Fang, Nanocomposites based on 3D macroporous biomass carbon with SnS_2 nanosheets hierarchical structure for efficient removal of hexavalent chromium, Chem. Eng. J. 369 (2019) 1138-1149.

[56] X. Li, W. Xu, M. Tang, L. Zhou, B. Zhu, S. Zhu, J. Zhu, Graphene oxide-based efficient and scalable solar desalination under one sun with a confined 2D water path, Proc. Natl. Acad. Sci. 113(49) (2016) 13953-13958.

[57] X. Wu, L. Wu, J. Tan, G.Y. Chen, G. Owens, H. Xu, Evaporation above a bulk water surface using an oil lamp inspired highly efficient solar-steam generation strategy, J. Mater. Chem. A 6(26) (2018) 12267-12274.

[58] Y. Wang, X. Wu, B. Shao, X. Yang, G. Owens, H. Xu, Boosting solar steam generation by structure enhanced energy management, Sci. Bull. (2020). https://doi.org/10.1016/j.scib.2020.04.036

[59] J. Liu, Q. Liu, D. Ma, Y. Yuan, J. Yao, W. Zhang, H. Su, Y. Su, J. Gu, D. Zhang, Simultaneously achieving thermal insulation and rapid water transport in sugarcane stems for efficient solar steam generation, J. Mater. Chem. A 7(15) (2019) 9034-9039.

[60] P. Sun, W. Zhang, I. Zada, Y. Zhang, J. Gu, Q. Liu, H. Su, D. Pantelic, B. Jelenkovic, D. Zhang, 3D-structured carbonized sunflower heads for improved energy efficiency in solar steam generation, ACS Appl. Mater. **Interfaces** 12(2) (2020) 2171-2179.

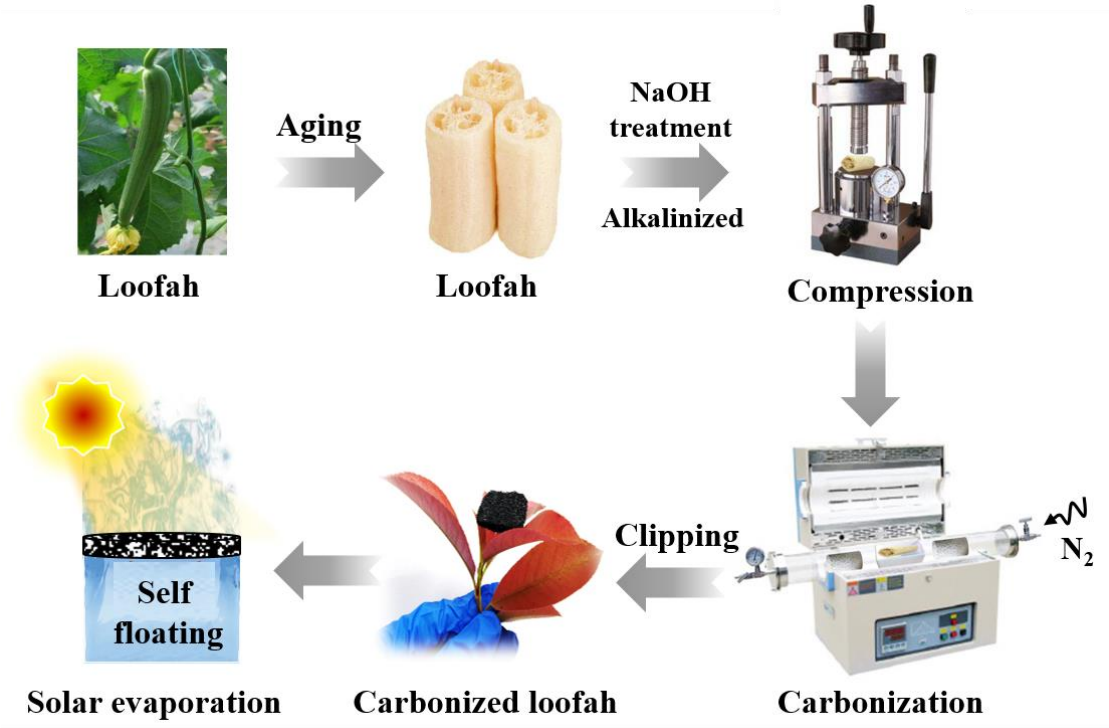
[61] C. Chen, Y. Li, J. Song, Z. Yang, Y. Kuang, E. Hitz, C. Jia, A. Gong, F. Jiang, J.Y. Zhu, B. Yang, J. Xie, L. Hu, Highly flexible and efficient solar steam generation device, Adv. Mater. 29(30) (2017) 1701756.

[62] M. Zhu, Y. Li, F. Chen, X. Zhu, J. Dai, Y. Li, Z. Yang, X. Yan, J. Song, Y. Wang, E. Hitz, W. Luo, M. Lu, B. Yang, L. Hu, Plasmonic wood for high-efficiency solar steam generation, Adv. Energy Mater. 8(4) (2018) 1701028.

[63] M. Zhu, J. Yu, C. Ma, C. Zhang, D. Wu, H. Zhu, Carbonized daikon for high efficient solar steam generation, Sol. Energy Mater. Sol. Cells 191 (2019) 83-90.

[64] Y. Bian, Q. Du, K. Tang, Y. Shen, L. Hao, D. Zhou, X. Wang, Z. Xu, H. Zhang, L. Zhao, S. Zhu, J. Ye, H. Lu, Y. Yang, R. Zhang, Y. Zheng, S. Gu, Carbonized bamboos as excellent 3D solar vapor-generation devices, Adv. Mater. Technol.-US 4(4) (2018) 1800593.

[65] Y. Chen, Y. Shi, H. Kou, D. Liu, Y. Huang, Z. Chen, B. Zhang, Self-floating carbonized tissue membrane derived from commercial facial tissue for highly efficient solar steam generation, ACS Sustain. Chem. Eng. 7(3) (2019) 2911-2915.



Scheme 1. Schematic illustration of preparation of carbonized loofah sponge for solar driven evaporation.

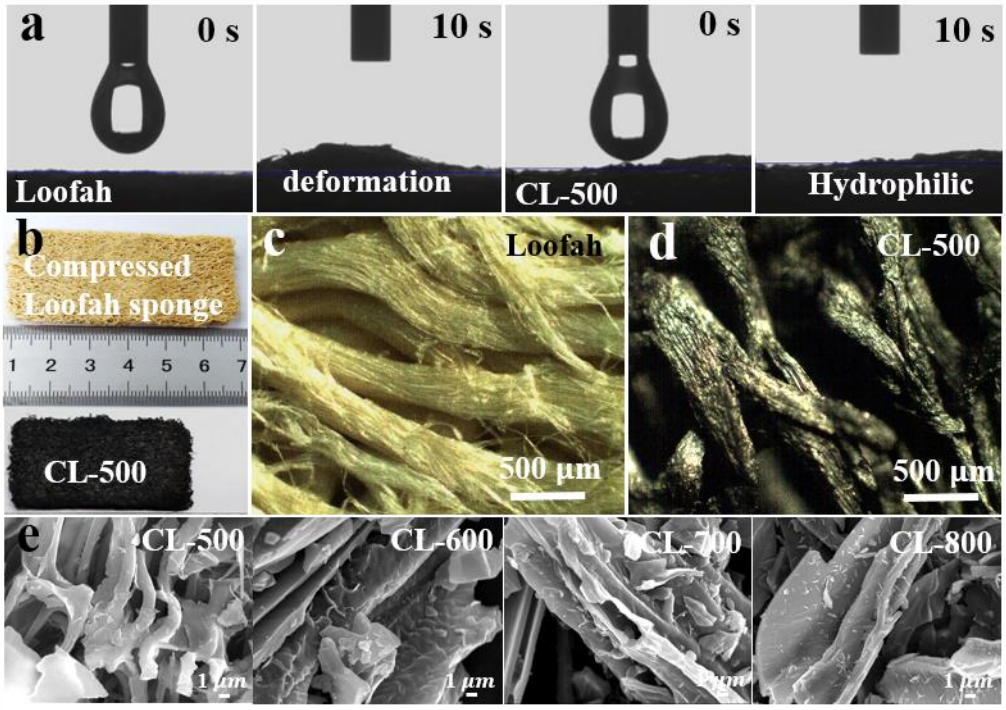


Fig. 2. (a) The pictures of surface hydrophilicity measurement. (b) Photographs of the compressed loofah sponge and CL-500 sponge. (c) and (d) Optical microscopy images of natural loofah sponge and CL-500 sponge. (e) SEM images of carbonized loofah sponges (CL-500, CL-600, CL-700, CL-800).

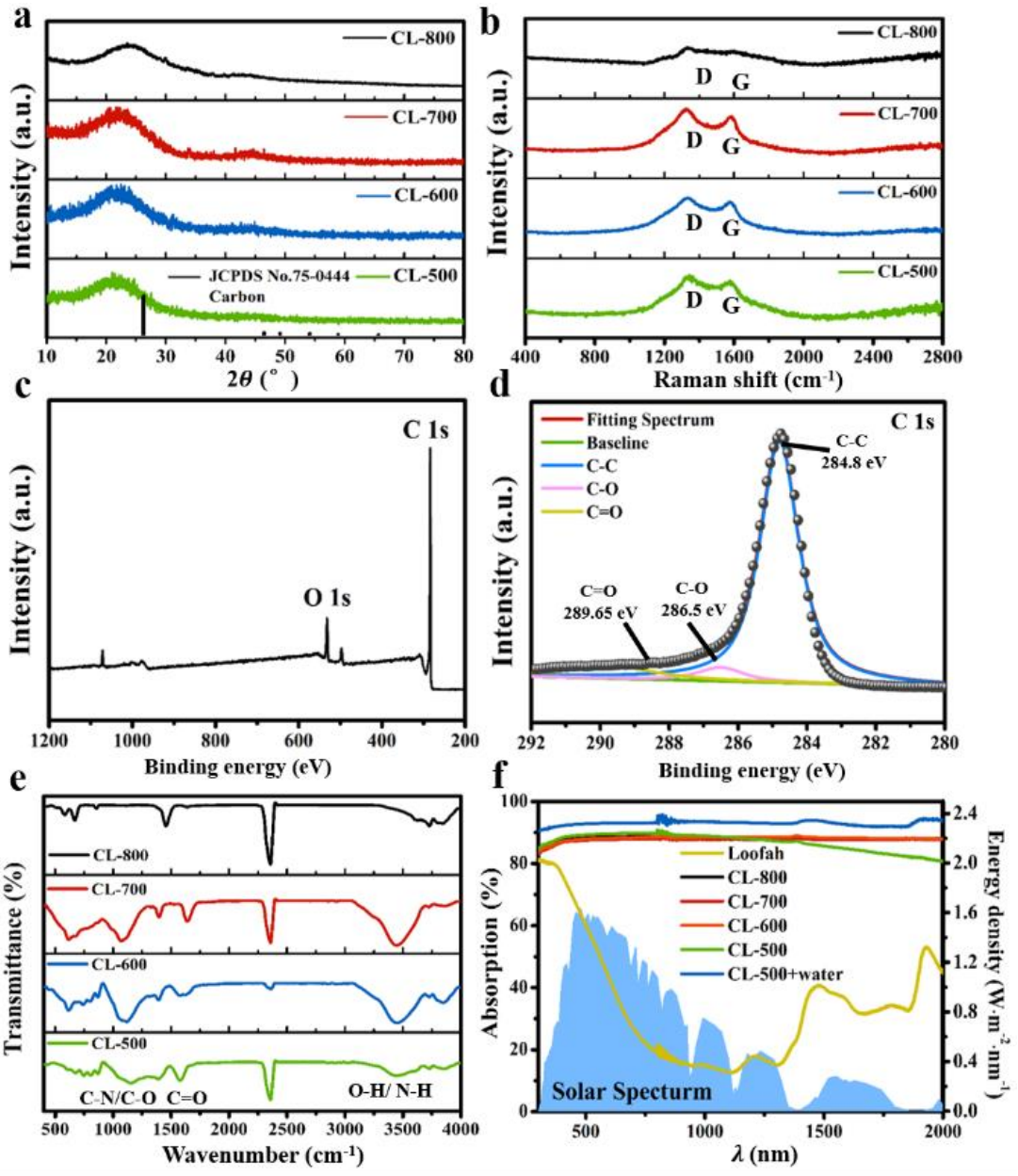


Fig. 3. (a) XRD patterns and (b) Raman spectra of the CL sponges. (c) XPS spectra of CL-500, and (d) high-resolution C1s of CL-500. (e) FTIR and (f) solar absorption spectra of the CL sponges carbonized at different temperatures.

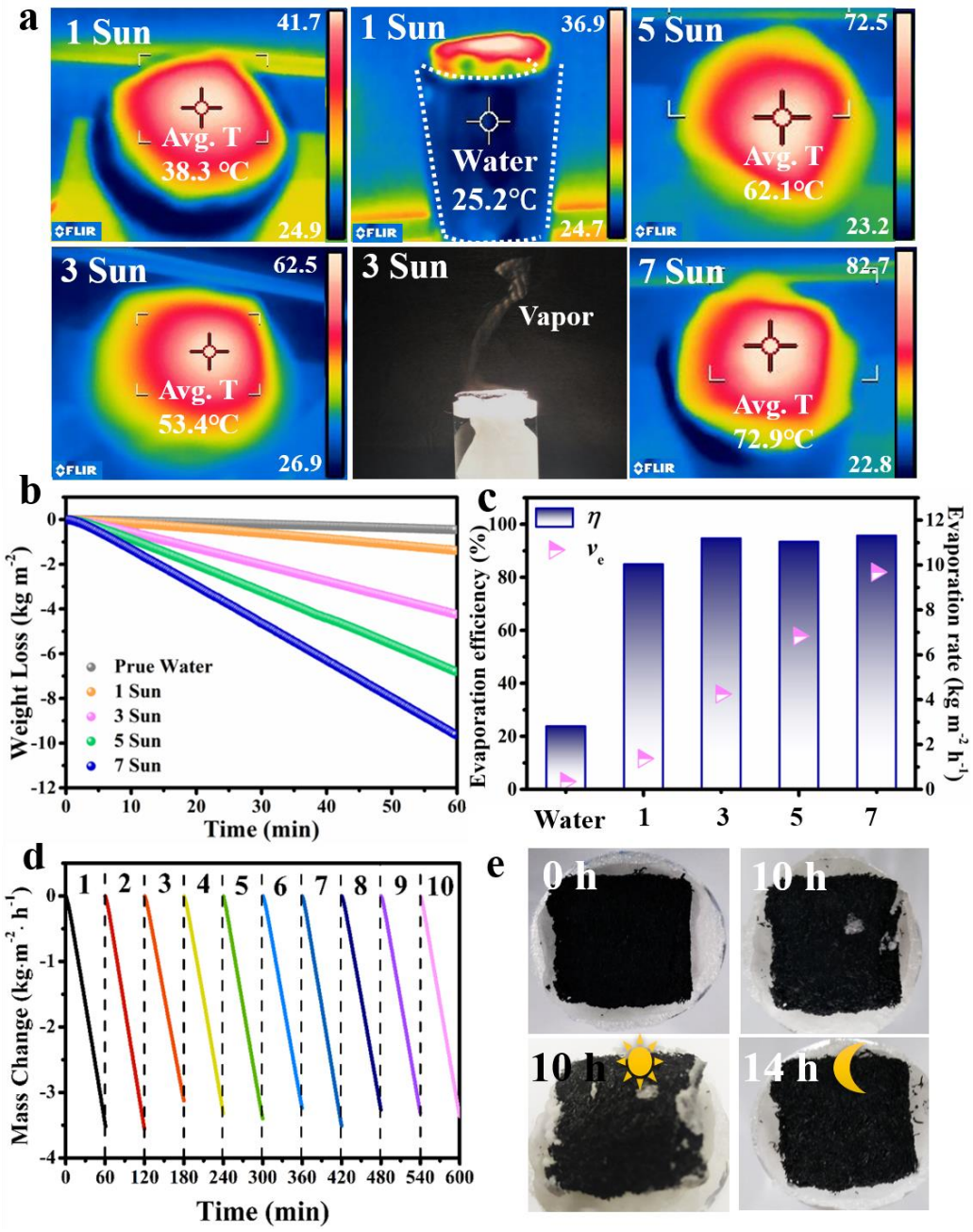


Fig. 4. Solar evaporation performance of the CL+PS evaporator. (a) IR images and digital photograph of the CL-500 sponge under different solar illuminations. (b) Real-time water mass loss, (c) solar evaporation rate and the corresponding solar evaporation efficiency of the blank water and CL-500 at different solar illuminations. (d) The stability of solar evaporation performance in seawater (3.5 wt% salinity) for 10 cycles under 3.0 Sun. (e) Photographs of the initial CL-500, the salt on the surfaces of the CL-500 sponges after 10 h solar evaporation under 3.0 Sun, and the self-desalting performance in the dark overnight.

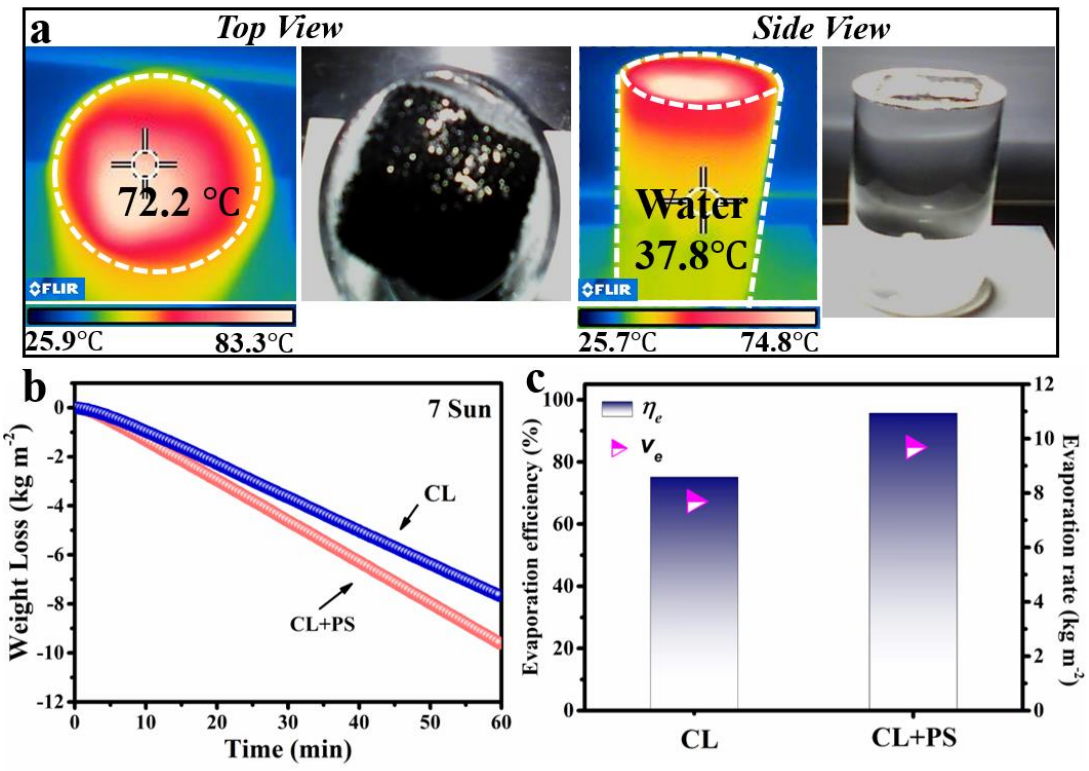


Fig. 5. The solar evaporation performance of the sole CL-500 sponge. (a) Infrared images and photos of the CL-500 sponge and bulk water, (b) the water weight loss over time, and (c) the corresponding evaporation rates and solar evaporation efficiency of the blank water, CL and CL+PS evaporator under 7.0 sun irradiation.

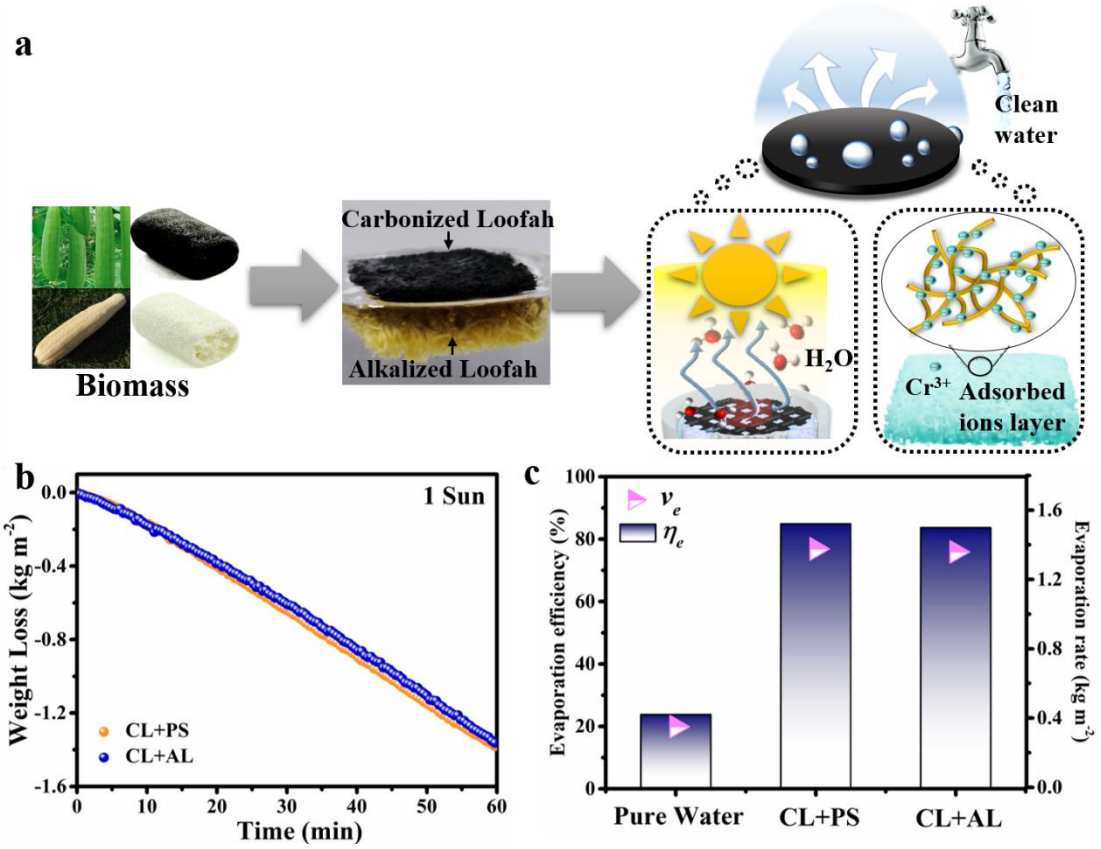


Fig. 6. Solar evaporation performance of the CL+AL evaporator. (a) Schematic illustration of the synergistic effect of solar evaporation and heavy metal ions adsorption by the CL+AL evaporator. (b) The water mass loss over time, (c) and the corresponding solar evaporation rates and energy efficiency of the pure water, CL+PS, and CL+AL evaporators under 1.0 Sun.

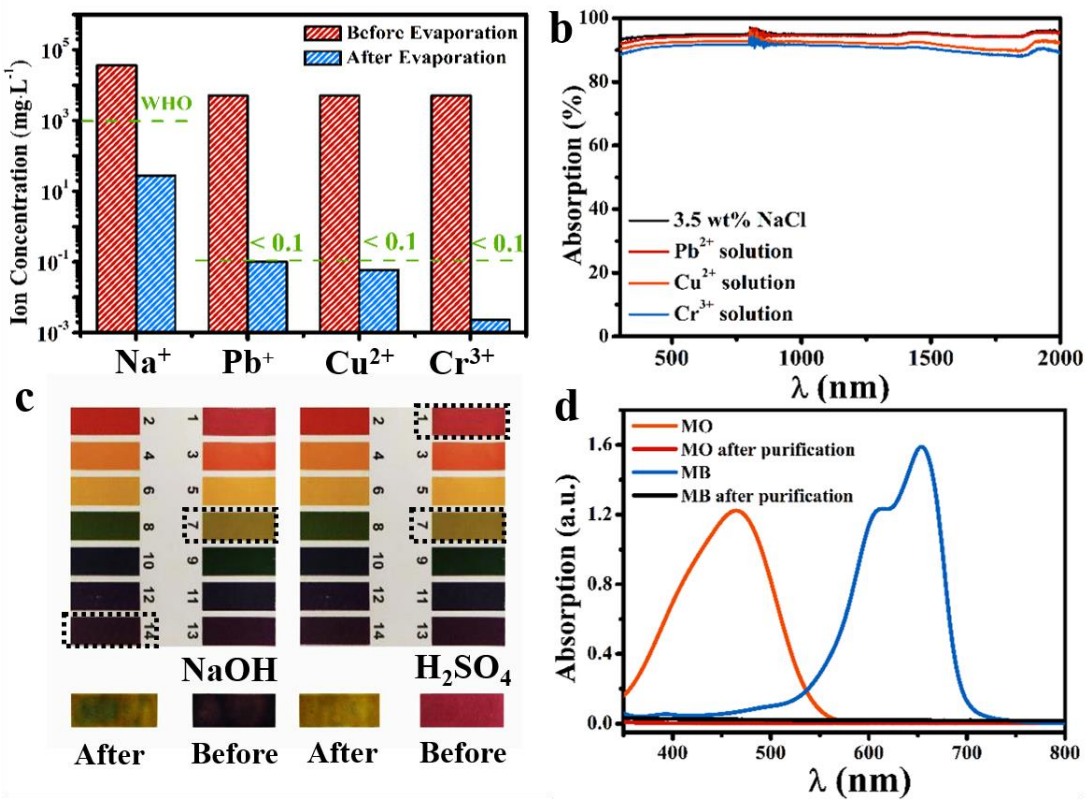


Fig. 7. (a) Measured concentrations of four ions in the simulated seawater and wastewater before and after solar evaporation. The dotted lines refer to the WHO standards for drinkable water. (b) The solar absorptivity of CL-500 sponge evaporator after being floated in average salinity of 3.5 wt% seawater and various heavy metal ions (Pb^{2+}, Cu^{2+}, Cr^{3+}) solutions for solar evaporation. (c) The pH values of condensed water evaporated from NaOH and H_2SO_4 solutions (1 mol/L). (d) The UV-vis absorption spectra of organic dyes in wastewater and condensed water after solar evaporation.

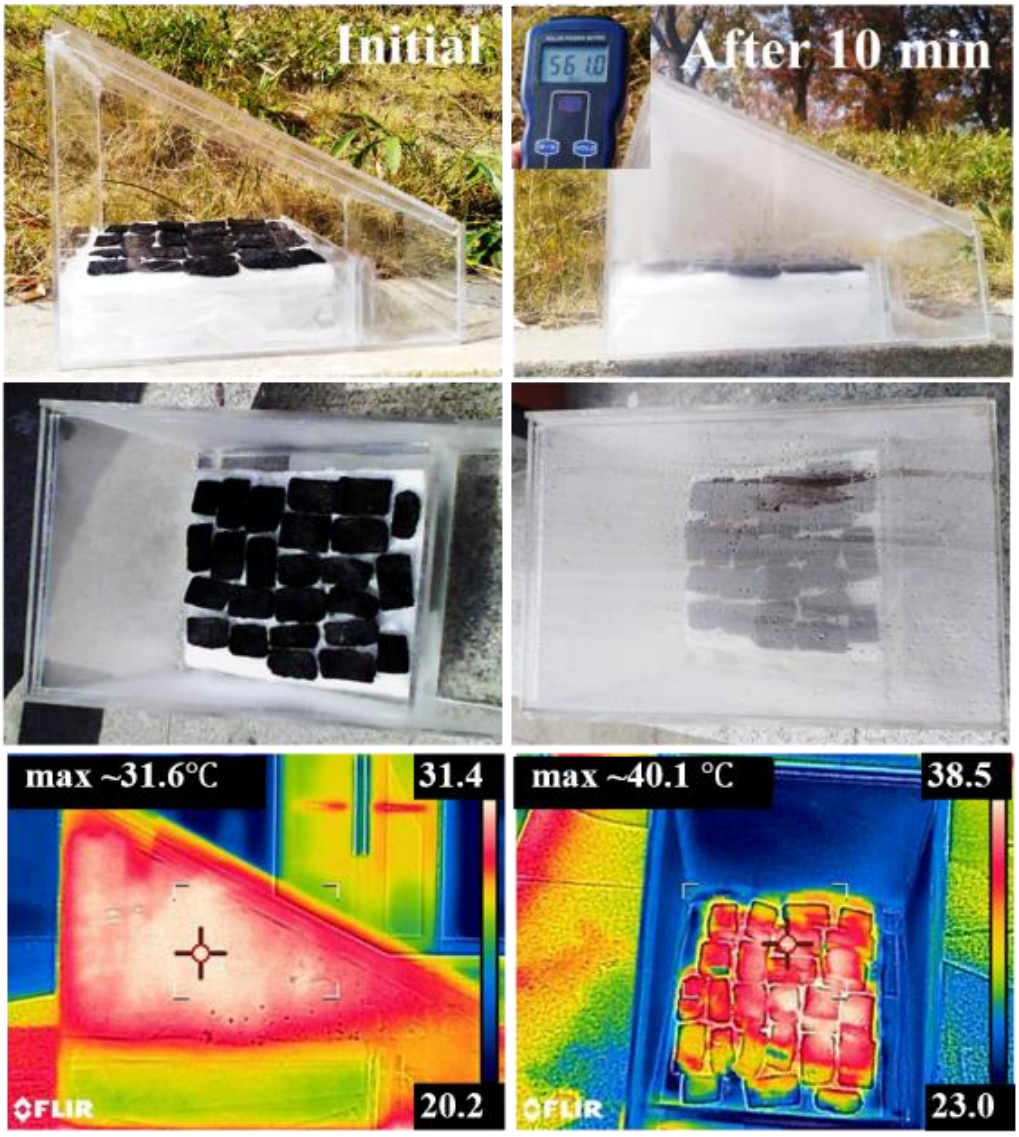
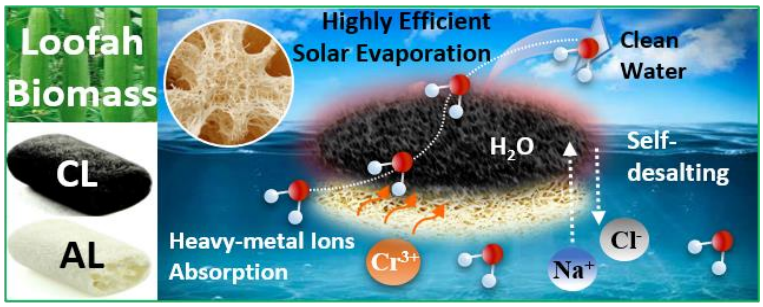


Fig. 8. The outdoor test (November, winter in Nanjing) using CL-500 sponge in an evaporation chamber made of transparent polymethyl methacrylate plastic plates. The photos, in order from left to right in the first row, corresponding to t = 0, 10 min solar illumination outdoors elucidate the solar evaporation, and the IR images display temperature distribution in the device.

Table 1. Solar evaporation performance of different biomass-based materials under 1.0 Sun

Evaporator	Evaporation rate [kg^{-1} m^{-2} h^{-1}]	Efficiency	Ref.
Surface-carbonized de-sugaring stems of sugarcane	1.57	87.4%	[59]
Carbonized mushrooms	1.475	78%	[45]
Carbonized sunflower heads	1.51	100.4%	[60]
Carbonized carrot	2.04	128%	[47]
Carbonized wood with holes	1.04	75%	[39]
Carbon nanotube modified flexible wood	0.95	65%	[61]
Plasmonic wood	—	68%	[62]
Mesoporous Wood	1.15	80%	[43]
Carbonized daikon	1.57	85.9%	[63]
Carbonized bamboo	1.547	62.3%	[64]
Carbonized lotus seedpods	1.3	86.5%	[51]
Carbonized Tissue	—	64%	[65]
CL+PS	1.38	85.5	Our work
CL+AL	1.36	83.7%	

Graphical Abstract



The loofah sponge-based solar evaporator, which is cost-effective and environmentally friendly, exhibits the synergic functions of solar evaporation and heavy metal ions adsorption. The carbonized loofah acts as the light absorber and delivers excellent self-desalting performance and high evaporation rate of 1.36 kg m^{-2} h^{-1} with corresponding energy efficiency of 83.7% under 1.0 Sun, while the alkalized loofah sponge can rapidly transport water and adsorb Cr^{3+} ions simultaneously.